Dynamic Behavior Modeling of Natural Rubber/Polybutadiene Rubber-Based Hybrid Magnetorheological Elastomer Sandwich Composite Structures

Ahobal .N , Lakshmi Pathi J * , Sakthivel G , Mohanraj Thangamuthu , Jegadeeshwaran Rakkiyannan * , Yogesh Jayant Bhalerao

Posted Date: 20 October 2023

doi: 10.20944/preprints202310.1282.v1

Keywords: Hybrid MRE; Sandwich structures; Smart structures; Dynamic Behavior Modeling; Vibration; Polymer composites

Article

Dynamic Behavior Modeling of Natural Rubber/Polybutadiene Rubber-Based Hybrid Magnetorheological Elastomer Sandwich Composite Structures

Ahobal N [1,3], Lakshmi Pathi J [2,*], Sakthivel G [3], Mohanraj T [4], Jegadeeshwaran R [2,*] and Y.J. Bhalerao [5]

[1] Department of Mechanical Engineering, Dayananda Sagar College of Engineering, Bengaluru, India.
[2] Centre for Automation, Vellore Institute of Technology, Chennai, India.
[3] School of Mechanical Engineering, Vellore Institute of Technology, Chennai, India.
[4] Department of Mechanical Engineering, Amrita School of Engineering, Amrita Vishwa Vidyapeetham, Coimbatore, India.
[5] Department of Mechanical Engineering and Design, School of Engineering, University of East Anglia, Norwich Research Park, Norwich NR47TIJ, United Kingdom.
* Correspondence: lakshmipathi@vit.ac.in; jegadeeshwaran.r@vit.ac.in.

Abstract: This study investigates the dynamic characteristics of Natural Rubber (NR)/Polybutadiene Rubber (PBR) based hybrid magnetorheological elastomer (MRE) sandwich composite beams through numerical simulations and finite element analysis, employing Reddy's third-order shear deformation theory. Four distinct hybrid MRE sandwich configurations were examined. The validity of finite element simulations was confirmed by comparing them with results from magnetorheological (MR) fluid-based composites. Further, parametric analysis explored the influence of magnetic field intensity, boundary conditions, ply orientation, and core thickness on beam vibration responses. Results reveal a notable 10.4% enhancement in natural frequencies in SC4-based beams under a 600mT magnetic field with clamped-free boundary conditions, attributed to increased PBR content in MR elastomer cores. However, higher magnetic field intensities result in slight frequency decrements due to filler particle agglomeration. Additionally, augmenting magnetic field intensity and magnetorheological content under clamped-free conditions improves the loss factor by 66% to 136%, presenting promising prospects for advanced applications. This research contributes to a comprehensive understanding of dynamic behavior and performance enhancement in hybrid MRE sandwich composites, holding significant implications for engineering applications. Furthermore, this investigation provides valuable insights into the intricate interplay between magnetic field effects, composite architecture, and vibration response.

Keywords: hybrid MRE; sandwich structures; smart structures; dynamic behavior modeling; vibration; polymer composites

1. Introduction

Advances in aerospace technology have led to the development of composite materials that feature properties that rival or even surpass those of traditional materials, notably fiber-reinforced polymers (FRPs). FRPs are renowned for their remarkable attributes, including a high strength-to-weight ratio, exceptional durability, stiffness, and resistance to corrosion, wear, and impact. However, these high-performance FRP composite structures face a formidable challenge—vibrations induced by dynamic loads. These vibrations often lead to resonance conditions and the risk of catastrophic failures, exacerbated by insufficient damping characteristics. In response to these critical challenges, the development of smart materials has emerged as alternative materials aimed at enhancing the performance, structural integrity, and overall comfort of composite structures. Among

 doi:10.20944/preprints202310.1282.v1

these smart materials, MR materials have gained prominence due to their field-dependent rheological properties [1,2].

In the past decade, magneto-rheological materials have gained significant attention, surpassing electrorheological (ER) materials. This shift in interest is attributed to their superior yield strength, resilience to temperature variations, and tolerance to contaminants compared to ER fluids, making them ideal for controlling structural vibrations. Significant research endeavors have focused on evaluating both the properties and practical applications of MR fluids in the domain of structural vibration control [3,4]. However, the use of MR fluids is constrained by issues such as the accumulation of iron particles in the absence of a magnetic field and their relatively high production costs. While MR gels and grease offer exceptional performance, they are susceptible to issues like sedimentation, deposition, environmental pollution, and sealing problems [5–7]. In contrast, MR elastomers (MREs), featuring rubber as their matrix material, excel in surmounting these challenges. They exhibit swift and reversible transformations, tunable stiffness, and advantageous viscoelastic properties in response to magnetic field application [8]. MREs provide several advantages, including lower manufacturing costs and the absence of iron particle accumulation, making them an appealing choice for various engineering applications.

In the development of Magnetorheological Elastomers (MREs), the composition plays a pivotal role in shaping their characteristics. Chen et al. [9] emphasized the significant impact of both the applied magnetic field and the iron particle content on MRE damping properties, offering insights into the intricate interplay between magnetic field intensity and material composition. The essential structure of MREs, characterized by a matrix of rubber intricately mixed with dispersed magnetic particles, has been elucidated by various researchers [10,11], highlighting the critical role of this composite structure in shaping MRE behavior. Several variables come into play when molding the properties of MREs, including the choice of magnetic filler material, the matrix type, and the compatibility of the magnetic filler with the matrix. Typically, iron particles of diverse shapes and sizes, exhibiting ferromagnetic properties with high magnetic saturation and soft magnetic attributes, emerge as the preferred choice for MREs [9,12]. Furthermore, the exceptional magnetorheological performance of MREs can be attributed to the synergy between magnetic fillers and the matrix material [13]. Chen et al. has demonstrated that natural rubber-based MREs surpass silicone rubber-based counterparts across various properties, encompassing tear strength, tensile strength, resilience factor, and hardness [14]. Investigating isotropic synthetic rubber-based MREs, as shown by Gong et al., shows an impressive 26% enhancement in the Magnetorheological (MR) effect with the incorporation of 0.6 volume fraction of carbonyl iron (CI) particles. This enhancement undoubtedly signifies a marked improvement in the material's rheological behavior. However, it does introduce a trade-off as it entails a reduction in its elastic properties [15]. This reduction in elasticity could be of concern, especially in structural applications where the ability to isolate vibrations is of paramount importance. MREs with diminished elastic properties may struggle to meet the demands for the necessary stiffness and structural integrity required to safeguard the overall system's performance and reliability.

To overcome the limitations posed by reduced elastic properties in Magnetorheological Elastomers (MREs), extensive research has focused on incorporating various additives, including plasticizers, silane coupling agents, and nano-sized particles like carbon black, carbon nanotubes, and graphene [16–20]. These additives serve to enhance the mechanical properties of MREs by reinforcing the interfacial interactions between fillers and the elastomeric matrix; however, they are not exempt from significant challenges. One of these challenges lies in the propensity of these fillers, particularly when in nano-sized forms, to agglomerate within the elastomeric matrix [21]. This phenomenon not only complicates the manufacturing process but also escalates costs, particularly in the case of nanomaterials [22]. Ensuring compatibility between the chosen fillers and the matrix material, as well as addressing processing intricacies and potential health and environmental concerns, emerges as crucial considerations in MRE development. Achieving the delicate equilibrium between attaining desired properties and managing these inherent limitations constitutes a challenging task.

 doi:10.20944/preprints202310.1282.v1

Consequently, researchers are compelled to explore novel materials and innovative techniques continually, with the aim of optimizing MRE composites for a diverse array of applications.

In recent years, researchers have embarked on an exploration of the untapped potential within hybrid matrix Magnetorheological Elastomer (MRE) composites, aiming to conquer the persistent challenges posed by nanofillers and the relatively modest mechanical properties inherent in conventional MREs. This innovative approach has opened up a promising pathway for addressing these challenges associated with nanofillers and the relatively low mechanical properties observed in conventional MREs [23–25].

Researchers aimed to find a balance between the mechanical performance and Magnetorheological (MR) effect by using NR and PBR by addressing a common challenge in MRE development. NR-based MREs excel in mechanical properties but often fall short in terms of the required MR effect for industrial applications. In contrast, PBR-based MREs exhibit a high MR effect but suffer from inferior mechanical properties. The synergy between NR's excellent synthetic mechanical performance and PBR's desirable characteristics, including high elasticity, low heat buildup, cold resistance, and flex fatigue resistance, allows for the development of hybrid matrices that capitalize on the strengths of both materials. This harmonious blend results in improved compatibility, as NR and PBR share active cross-linking spots and possess similar vulcanization mechanisms and curing rates [26]. Song et al. research reveals that increasing polybutadiene rubber (PBR) content from 10% to 50% results in a minor decrease in the zero-field modulus, accompanied by a substantial enhancement in magneto-rheological (MR) effect, ranging from 31.25% to 44.19% [26]. This work underscores the trade-off between these critical material properties in hybrid MREs, with implications for future applications. Several works on matrix materials incorporating blends of NR/ styrene-butadiene rubber (SBR) and NR/ nitrile butadiene rubber (NBR) reveals the improved mechanical properties when compared to matrix composed of only NR or NBR [27]. Pal et al. showed the blends of Urethane Rubber (UR)/NR and PBR/NR exhibited 35-40% enhancement in mechanical properties [28]. The study by Ge et al. revealed that the incorporation of rosin glycerin ester into natural rubber/rosin glycerin hybrid matrix-based MREs resulted in an increase in the zero-field modulus (G_0) at a 9% concentration, but this effect diminished at higher concentrations. Furthermore, an increase in carbon iron (CI) content led to a substantial 575% improvement in G_0 at 80 wt%. Additionally, the application of a magnetic field intensified inter-particle forces within CI-based MREs, highlighting the potential for tailoring the mechanical properties of these materials for diverse engineering applications [29].

Previous research into hybrid matrix MREs has shown limited progress in comprehending their mechanical, rheological properties and dynamic behavior. There exists a clear absence of both mathematical approaches and experimental investigations in analyzing the dynamic behavior of hybrid MRE composites. In the present study, the dynamic characteristics of NR/PBR-based hybrid magnetorheological (MR) elastomer sandwich composite beams are investigated using numerical simulations. This investigation considers various compositions of NR and PBR to develop finite element equations for the sandwich composite beam. The potential energy and kinetic energy equations for the hybrid elastomer sandwich composite beam with FRP face sheets, employing Reddy's third-order shear deformation theory, are derived. Remarkably, there is a lack of research on the dynamic study of hybrid MRE sandwich composite structures. To address this gap, the governing differential equations of motion for the hybrid MRE sandwich composite beam are established, considering various compositions of the NR/PBR matrix. These equations are presented using a three-node line element with five degrees of freedom at each node. To validate the finite element simulations, the results are compared with existing data on MR fluids available in the literature. Additionally, the study examines the dynamic characteristics of various configurations of hybrid MRE sandwich composite beams under the influence of magnetic field intensity, ply orientation, core thickness, and boundary conditions. Figure 1 outlines the various steps involved in the numerical simulation of hybrid MRE sandwich composites, representing a concerted effort to gain a deeper understanding of the characteristics of these structures.

Preprints (www.preprints.org) | NOT PEER-REVIEWED | Posted: 20 October 2023 doi:10.20944/preprints202310.1282.v1

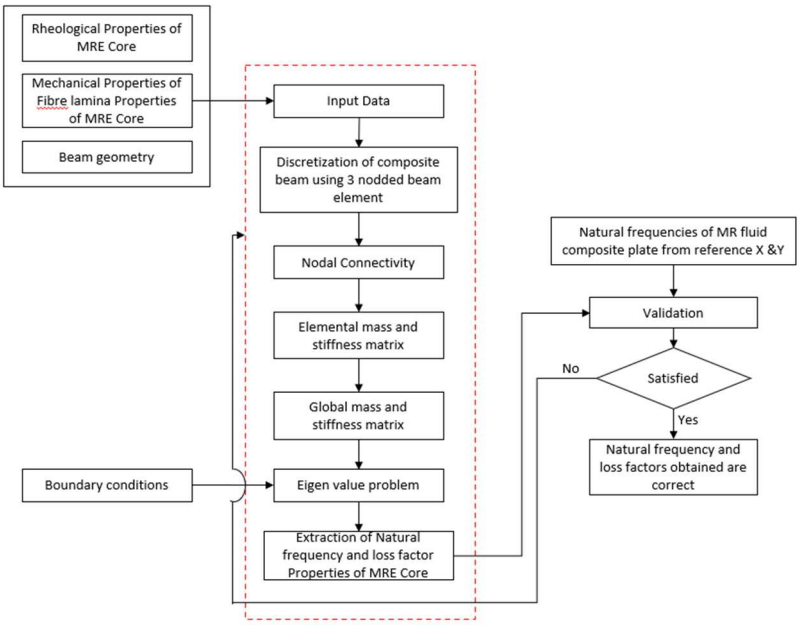

Figure 1. Steps involved in numerical investigation.

2. Mathematical Modelling

Sandwich composite structures with laminated face sheets, as shown in Figure 2, are used in various high-performance engineering applications, such as aircraft wings, windmill blades, and helicopter rotor blades, due to their exceptional structural characteristics. These composite structures consist of a core composed of Carbonyl iron Powder (CIP), a magnetic filler material uniformly dispersed in a hybrid MR elastomer core comprising both PBR (polybutadiene rubber) and NR (natural rubber). Flanking this core are multi-layered face sheets made of glass fiber-reinforced polymer. In the analysis, perfect bonding between all three layers of the sandwich composite beam is assumed. To comprehensively explore the dynamic properties of these composite beams, four distinct configurations of hybrid MR elastomers, denoted as SC1, SC2, SC3, and SC4, are considered. The composition of these hybrid elastomers is detailed in Table 1, where the proportions of PBR mixed with NR are determined following the approach outlined by Song et al. [26]. The geometric parameters of the sandwich composite beam include the length and width of the face sheets, represented as 'L' and 'w', respectively. Additionally, we define the thicknesses of the elastomer core, bottom face sheet, and top face sheet as 'h_c', 'h_b', and 'h_t', respectively.

Table 1. Composition of MR Elastomer core samples.

Materials	SC1	SC2	SC3	SC4
PBR	10	30	50	100
NR	90	70	50	0
Carbonyl Iron (CIP)	190	190	190	190
Cumarone	12	12	12	12
ZnO	5	5	5	5
4010NA	2	2	2	2
RD	3	3	3	3
Sulphur	3	3	3	3
SA	1	1	1	1
CZ	0.5	0.5	0.5	0.5

PBR: polybutadiene rubber; NR: natural rubber; CZ: n-cyclohexyl-2 benzothiazole sulfonamide; RD: poly(1, 2-dihydro-2, 2, 4-trimethyl-quinoline); ZnO: zinc oxide; SA: stearic acid .

Preprints (www.preprints.org) | NOT PEER-REVIEWED | Posted: 20 October 2023 doi:10.20944/preprints202310.1282.v1

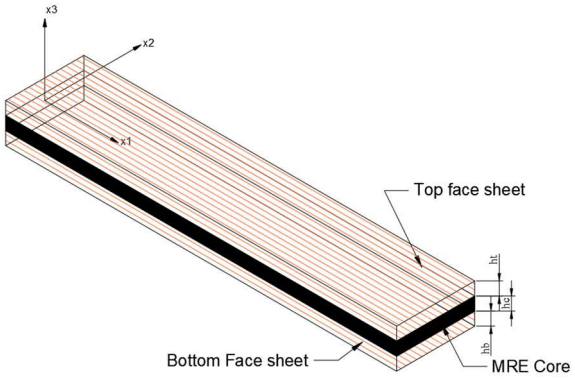

Figure 2. Dimensions of Sandwich composite beam.

2.1. Modelling of face sheets

The governing differential equations of motion for the sandwich composite beam were formulated using Reddy's third-order shear deformation theory (RTSDT). RTSDT incorporates shear deformation effects by assuming that the deformation field of the skin layers varies as a third order function of x_3, representing the thickness coordinate of the sandwich composite beam. This theory provides a more accurate description of the displacement field for the face sheets of the sandwich composite beam, and its formulation is as follows:

$$\begin{gathered} {u_1}^j(x_1, x_3, t) = {u_1}_0^j(x_1, t) + x_3\varphi(x_1, t) + {x_3}^2\theta(x_1, t) + {x_3}^3\emptyset(x_1, t) \qquad j = t, b \\ {u_3}^j(x_1, x_3, t) = {u_3}_0^j = {u_3}_0 \end{gathered} \tag{1}$$

The displacements along the x_1 −axis for the first and third layers, as well as the transverse deflection along the x_3 −direction, are denoted as ${u_1}^j$ and ${u_3}^j$, respectively. It is assumed that the transverse deflection for the first and third layers is equal. Furthermore, considering that the bottom and top layers of the composite beam are traction-free, the boundary conditions can be expressed as follows:

$$\tau_{x_1x_3}^j\left(x_1, \pm\frac{h_j}{2}, t\right) = 0 \tag{2}$$

To account for the assumed traction-free boundary condition of the beam, we can simplify the displacement parameters by eliminating the second-order terms. Following this reduction, the resulting displacement field, which contains third-order terms, is given as follows:

$$\begin{gathered} {u_1}^j(x_1, x_3, t) = {u_1}_0^j(x_1, t) + x_3\varphi(x_1, t) - \frac{4{x_3}^3}{3{h_j}^2}\zeta \\ \zeta = \left(\frac{\partial {u_3}_0^j}{\partial x_1} + \varphi\right) \end{gathered} \tag{3}$$

The transverse term about the x_1 −axis is represented as φ, while the wrapping term ζ is expressed in terms of the transverse plane rotation. The strain-displacement relationship for the face sheets of the sandwich composite beam, derived using the small strain theory, is as follows:

$$\begin{gathered} \varepsilon_{x_1}^j = \varepsilon_0^j + x_3\varepsilon_1^j + {x_3}^3\varepsilon_3^j, \\ \gamma_{x_1x_3}^j = \gamma_0^j + {x_3}^2\gamma_2^j \end{gathered} \tag{(4}$$

where,

$$\begin{gathered} \varepsilon_0^j = \frac{\partial {u_1}_0^j}{\partial x_1},\ \varepsilon_1^j = \frac{\partial \varphi}{\partial x_1},\ \varepsilon_3^j = -k_1\frac{\partial \zeta}{\partial x_1} \\ \gamma_0^j = \zeta, \gamma_2^j = -k_2\zeta \end{gathered} \tag{(5}$$

Where in, $k_1 = 4/3{h_j}^2$ and $k_2 = 3k_1$. The resultant force and moments of the sandwich composite beam which are analogous with the strain terms given in equation 4 is represented as

$$\{N^j\} = [ABD]\{\varepsilon^j\} \tag{6}$$

Preprints (www.preprints.org) | NOT PEER-REVIEWED | Posted: 20 October 2023 doi:10.20944/preprints202310.1282.v1

where $\{N^j\}$ matrix includes bending moment, in-plane force, transverse shear and higher order shear force resultants, and higher order moments. $[ABD]$ matrix contains terms of transverse shear stiffness, bending stiffness, extensional stiffness, extensional–bending stiffness, higher order transverse shear stiffness and extensional bending which are given in equation-(i) of appendix-I.

2.2. Modelling of MR Elastomer Core

In the modeling of Magnetorheological Elastomers (MREs), it is presumed that the normal stresses developed within the MR elastomer core are negligible due to its significantly lower elastic modulus compared to the face sheets. Additionally, a no-slip condition is assumed at the interface between the face sheets and the MR elastomer core, simplifying the boundary conditions. To facilitate the modeling process, the longitudinal deformation (${u_1}^c$) and transverse shear strain (γ^c) of the elastomer core are derived from the kinematics of the deformed elastomer, providing essential parameters for the construction of a comprehensive MRE model.

$$\begin{aligned} {u_1}^c &= \frac{{u_1}^t - {u_1}^b}{2} + \left(\frac{h_b - h_t}{4}\right)\varphi + \left(\frac{h_b - h_t}{12}\right)\zeta \\ \gamma^c &= \frac{{u_1}^t - {u_1}^b}{h_c} - \left(\frac{h_t + h_b}{2h_c}\right)\varphi + \left(\frac{h_t + h_b}{6h_c}\right)\zeta + \frac{\partial u_{3_0}}{\partial x_1} \end{aligned} \tag{7}$$

The resultant shear force associated with MR elastomer core is expressed as

$$Q^c = G'_{xz} h_c \gamma^c \tag{8}$$

where G'_{xz} is complex shear modulus of constraining layer which is expressed as

$$G'_{xz} = G^*(1 + i\eta) \tag{9}$$

2.3. Kinetic and Strain Energy Formulations

The strain energy (δU) attributed to the virtual displacements in the NR/BR hybrid MR elastomer sandwich composite beam with face sheets can be expressed as follows:

$$\delta U = \int w \left(\sum_{j=t,b} \left(N^j \delta\varepsilon_0^j + M^j \delta\varepsilon_1^j - k_1 \delta P^j \varepsilon_3^i + Q^j \delta\gamma_0^j - k_2 R^j \delta\gamma_2^j \right) + R^c \delta\gamma^c \right) dx_1 \tag{10}$$

Furthermore, the strain energy is reduced in relation to the deformation field as

Preprints (www.preprints.org) | NOT PEER-REVIEWED | Posted: 20 October 2023 doi:10.20944/preprints202310.1282.v1

$$
\begin{aligned}
\delta U = \int w \Bigg[\sum_{j=t,b} \Bigg(& A \frac{\partial {u_1}_0^j}{\partial x_1} + B \frac{\partial \varphi}{\partial x_1} - E k_1 \frac{\partial \zeta}{\partial x_1} \Bigg) \frac{\partial \delta {u_1}_0^j}{\partial x_1} \\
& + \left(B \frac{\partial {u_1}_0^j}{\partial x_1} + D \frac{\partial \varphi}{\partial x_1} - E k_1 \frac{\partial \zeta}{\partial x_1} \right) \frac{\partial \delta \varphi}{\partial x_1} \\
& + \left(E \frac{\partial {u_1}_0^j}{\partial x_1} + F \frac{\partial \varphi}{\partial x_1} + H k_1 \frac{\partial \zeta}{\partial x_1} \right) k_1 \frac{\partial \delta \zeta}{\partial x_1} \\
& + \left(A_s \left(\frac{\partial {u_3}_0^j}{\partial x_1} + \varphi \right) + k_2 D_s \zeta \right) \left(\frac{\partial \delta {u_3}_0^j}{\partial x_1} + \delta \varphi \right) \\
& + \left(D_s \left(\frac{\partial {u_3}_0^j}{\partial x_1} + \varphi \right) + k_2 F_s \zeta \right) k_2 \delta \zeta \Bigg] dx_1 \\
& + \int w h_c G_s \Bigg[\left(\frac{\partial {u_3}_0^i}{\partial x_1} \right) \left(\frac{\partial \delta {u_3}_0^i}{\partial x_1} \right) \\
& + \left(\left(\frac{{u_1}^t - {u_1}^b}{h_c} \right) \left(\frac{\partial \delta {u_3}_0^j}{\partial x_1} \right) \right. \\
& \left. + \left(\frac{\delta {u_1}^t - \delta {u_1}^b}{h_c} \right) \left(\frac{\partial {u_3}_0^j}{\partial x_1} \right) \right) \\
& + \left(\frac{\delta {u_1}^t - \delta {u_1}^b}{h_c} \right) \left(\frac{{u_1}^t - {u_1}^b}{h_c} \right) \\
& - \left(\frac{h_t + h_b}{2 h_c} \right) \Bigg(\varphi \left(\frac{\partial \delta {u_3}_0^j}{\partial x_1} \right) + \delta \varphi \left(\frac{\partial {u_3}_0^j}{\partial x_1} \right) \\
& + \varphi \left(\frac{\delta {u_1}^t - \delta {u_1}^b}{h_c} \right) + \delta \varphi \left(\frac{{u_1}^t - {u_1}^b}{h_c} \right) \Bigg) \\
& + \left(\frac{h_t + h_b}{6 h_c} \right) \Bigg(\zeta \left(\frac{\partial \delta {u_3}_0^j}{\partial x_1} \right) + \delta \zeta \left(\frac{\partial {u_3}_0^j}{\partial x_1} \right) \\
& + \zeta \left(\frac{\delta {u_1}^t - \delta {u_1}^b}{h_c} \right) + \delta \zeta \left(\frac{{u_1}^t - {u_1}^b}{h_c} \right) \Bigg) \\
& + \left(\frac{h_t + h_b}{2 h_c} \right)^2 \varphi \delta \varphi \\
& - \left(\frac{h_t + h_b}{2 h_c} \right) \left(\frac{h_t + h_b}{6 h_c} \right) (\varphi \delta \zeta + \delta \varphi \zeta) \\
& + \left(\frac{h_t + h_b}{6 h_c} \right)^2 \zeta \delta \zeta \Bigg] dx_1
\end{aligned}
\tag{11}
$$

The kinetic energy (δK) resulting from the in-plane, transverse, and shear displacements of the structure is expressed as follows:

Preprints (www.preprints.org) | NOT PEER-REVIEWED | Posted: 20 October 2023 doi:10.20944/preprints202310.1282.v1

$$\delta K = \sum_{j=t,b} \int_{h_b^j}^{h_t^j} w\rho_f \Big[\Big(\big(\dot{u}_{1_0}^{\,j} + x_3\dot{\varphi} - k_1\dot{\zeta}\big)\big(\delta\dot{u}_{1_0}^{\,j} + x_3\delta\dot{\varphi} - k_1\delta\dot{\zeta}\big) + \dot{u}_{3_0}\delta\dot{u}_{3_0}\Big) + {x_3}^2\left(\frac{\partial \dot{u}_{3_o}^{\,j}}{\partial x_1} + \dot{\varphi} + k_2{x_3}^2\dot{\zeta}\right)\left(\frac{\partial \delta\dot{u}_{3_o}^{\,j}}{\partial x_1} + \delta\dot{\varphi} + k_2{x_3}^2\delta\dot{\zeta}\right)\Big] dx_1 dx_3 + \int_{-\frac{h_c}{2}}^{\frac{h_c}{2}} w\rho_c\big(\dot{u}_c\delta\dot{u}_c + \dot{u}_{3_0}\delta\dot{u}_{3_0} + {x_3}^2\dot{\gamma}^c\delta\gamma^c\big)\, dx_1 dx_3 \tag{12}$$

Further, the kinetic energy is reduced in the form of

$$\begin{aligned}\delta K = \sum_{j=t,b} \int_{h_b^j}^{h_t^j} w \Bigg[& \left(I_0\frac{\partial u_{1_0}^{\,j}}{\partial t} + I_1\frac{\partial\varphi}{\partial t} - I_3k_1\frac{\partial\zeta}{\partial t}\right)\frac{\partial\delta u_{1_0}^{\,j}}{\partial t} + \left(I_1\frac{\partial u_{1_0}^{\,j}}{\partial t} + I_2\frac{\partial\varphi}{\partial t} - I_4k_1\frac{\partial\zeta}{\partial t}\right)\frac{\partial\delta\varphi}{\partial t} \\ & + \left(I_3\frac{\partial u_{1_0}^{\,j}}{\partial t} + I_4\frac{\partial\varphi}{\partial t} + I_4k_1\frac{\partial\zeta}{\partial t}\right)k_1\frac{\partial\delta\zeta}{\partial t} + I_0\frac{\partial u_{3_0}^{\,j}}{\partial t}\frac{\partial\delta u_{3_0}^{\,j}}{\partial t} \\ & + \left(I_2\left(\frac{\partial u_{3_0}^{\,j}}{\partial t\partial x_1} + \varphi\right) + I_4k_2\frac{\partial\zeta}{\partial t}\right)\left(\frac{\partial\delta u_{3_0}^{\,j}}{\partial t\partial x_1} + \delta\varphi\right) \\ & + \left(I_4k_2\left(\frac{\partial u_{3_0}^{\,j}}{\partial t\partial x_1} + \varphi\right) + I_6{k_2}^2\frac{\partial\zeta}{\partial t}\right)\left(\frac{\partial\delta\zeta}{\partial t}\right)\Bigg] dx_1 \\ & + \int_{-\frac{h_c}{2}}^{\frac{h_c}{2}} \Bigg[wI_{0c}\left(\left(\frac{u_{1_0}^{\,t} + u_{1_0}^{\,b}}{2}\right)\left(\frac{\delta u_{1_0}^{\,t} + \delta u_{1_0}^{\,b}}{2}\right) + \frac{\partial u_{3_0}^{\,j}}{\partial t}\frac{\partial\delta u_{3_0}^{\,j}}{\partial t}\right) \\ & + I_{2c}\left(\frac{u_{1_0}^{\,t} + u_{1_0}^{\,b}}{2}\right)\left(\frac{\delta u_{1_0}^{\,t} + \delta u_{1_0}^{\,b}}{2}\right) \\ & - \left(\frac{h_t - h_b}{2h_2}\right)\Bigg(\left(\frac{\partial\varphi}{\partial t}\right)\left(\frac{\delta u_{1_0}^{\,t} + \delta u_{1_0}^{\,b}}{2}\right) + \left(\frac{\partial\delta\varphi}{\partial t}\right)\left(\frac{u_{1_0}^{\,t} + u_{1_0}^{\,b}}{2}\right) + \left(\frac{\partial\delta\varphi}{\partial t}\right)\left(\frac{\partial u_{3_0}^{\,j}}{\partial t\partial x_1}\right) \\ & + \left(\frac{\partial\varphi}{\partial t}\right)\left(\frac{\partial\delta u_{3_0}^{\,j}}{\partial t\partial x_1}\right)\Bigg) \\ & + \left(\frac{h_t - h_b}{6h_2}\right)\Bigg(\left(\frac{\partial\zeta}{\partial t}\right)\left(\frac{\delta u_{1_0}^{\,t} + \delta u_{1_0}^{\,b}}{2}\right) + \left(\frac{\partial\delta\zeta}{\partial t}\right)\left(\frac{u_{1_0}^{\,1} + u_{1_0}^{\,3}}{2}\right) + \left(\frac{\partial\delta\zeta}{\partial t}\right)\left(\frac{\partial u_{3_0}^{\,j}}{\partial t\partial x_1}\right) \\ & + \left(\frac{\partial\zeta}{\partial t}\right)\left(\frac{\partial\delta u_{3_0}^{\,j}}{\partial t\partial x_1}\right)\Bigg) + \left(\frac{u_{1_0}^{\,t} + u_{1_0}^{\,b}}{2}\right)\left(\frac{\partial\delta u_{3_0}^{\,j}}{\partial t\partial x_1}\right) + \left(\frac{\delta u_{1_0}^{\,t} + \delta u_{1_0}^{\,b}}{2}\right)\left(\frac{\partial u_{3_0}^{\,j}}{\partial t\partial x_1}\right) \\ & + \left(\frac{h_t - h_b}{2h_c}\right)^2\left(\frac{\partial\varphi}{\partial t}\right)\left(\frac{\partial\delta\varphi}{\partial t}\right) - \frac{1}{12}\left(\frac{h_t - h_b}{h_c}\right)^2\left(\left(\frac{\partial\varphi}{\partial t}\right)\left(\frac{\partial\delta\zeta}{\partial t}\right) + \left(\frac{\partial\delta\varphi}{\partial t}\right)\left(\frac{\partial\zeta}{\partial t}\right)\right) \\ & + \left(\frac{h_t - h_b}{6h_c}\right)^2\left(\frac{\partial\zeta}{\partial t}\right)\left(\frac{\partial\delta\zeta}{\partial t}\right)\Bigg] dx_1\end{aligned} \tag{13}$$

where $I_0, I_1, I_2, I_3, I_4, I_6$ are inertia terms are given in equation-(ii) of appendix-I.

The expression for the virtual work done (δV) due to the distributed transverse load $q(x,t)$ at time t is as follows:

$$\delta V = \int q\delta u_{3_0}\, dx_1 \tag{14}$$

Let δw_0 represent the virtual transverse deflection of the sandwich composite beam. When dealing with dynamic structures, it's important to establish that admissible virtual displacements are set to zero at two specific instances, denoted as t_1 and t_2, during which the precise position of the structure is known. To derive the variational functional, denoted as I, for the initial value problem, Hamilton's principle is employed as

Preprints (www.preprints.org) | NOT PEER-REVIEWED | Posted: 20 October 2023 doi:10.20944/preprints202310.1282.v1

$$
\begin{aligned}
I = \int_{t1}^{t2} \int \Bigg[& -\left(\frac{\partial N^{t}}{\partial x_1} - I_0 \ddot{u}_{1_0}^{t} - I_1 \ddot{\varphi} + k_1 I_3 \ddot{\xi}\right) \delta u_{1_0}^{b} - \left(\frac{\partial N^{b}}{\partial x_1} - I_0 \ddot{u}_{1_0}^{b} - I_1 \ddot{\varphi} + k_1 I_3 \ddot{\zeta}\right) \delta u_{1_0}^{b} \\
& - \left(\frac{\partial M^{t}}{\partial \partial x_1} + \frac{\partial M^{c}}{\partial x_1} - Q^{t} - Q^{b} - 2I_2 \ddot{\varphi} - I_1\left(\ddot{u}_{1_0}^{t} + \ddot{u}_{1_0}^{b}\right) + 2k_1 I_4 \ddot{\zeta}\right) \delta\varphi \\
& - \left(\frac{\partial Q^{t}}{\partial x_1} + \frac{\partial Q^{b}}{\partial x_1} + \frac{\partial Q^{c}}{\partial x_1} + q - I_0 \ddot{u}_{3_0}\right) \delta u_{3_0} \\
& - \left(-k_1 \frac{\partial P}{\partial x_1} + \frac{4R}{{h_j}^2} + k_1 I_3\left(\ddot{u}_{1_0}^{t} + \ddot{u}_{1_0}^{b}\right) + 2k_1 I_4 \ddot{\varphi} + {k_1}^2 I_6 \ddot{\zeta}\right) \delta\zeta \Bigg] dx_1 \, dt
\end{aligned} \tag{15}
$$

The governing differential equations of motion of the sandwich composite beam are attained by setting the coefficients of virtual displacements in the domain Ω to zero.

$$
\begin{aligned}
\delta u_{1_0}^{t}: \quad & \frac{\partial N^{t}}{\partial x_1} - I_0 \ddot{u}_{1_0}^{t} - I_1 \ddot{\varphi} + k_1 I_3 \ddot{\zeta} = 0 \\
\delta u_{1_0}^{b}: \quad & \frac{\partial N^{b}}{\partial x_1} - I_0 \ddot{u}_{1_0}^{b} - I_1 \ddot{\varphi} + k_1 I_3 \ddot{\zeta} = 0 \\
\delta\varphi: \quad & \frac{\partial M^{t}}{\partial x_1} + \frac{\partial M^{b}}{\partial x_1} - Q^{t} - Q^{b} - 2I_2 \ddot{\varphi} - I_1\left(\ddot{u}_{1_0}^{t} + \ddot{u}_{1_0}^{b}\right) + 2k_1 I_4 \ddot{\zeta} = 0 \\
\delta u_{3_0}: \quad & \frac{\partial Q^{t}}{\partial x_1} + \frac{\partial Q^{c}}{\partial x_1} + \frac{\partial Q^{b}}{\partial x_1} + q - I_0 \ddot{u}_{3_0} \\
\delta\zeta: \quad & -k_1\left(\frac{\partial P^{t}}{\partial x_1} + \frac{\partial P^{b}}{\partial x_1}\right) + \frac{4}{{h_j}^2}\left(R^{t} + R^{b}\right) + k_1 I_3\left(\ddot{u}_{1_0}^{t} + \ddot{u}_{1_0}^{b}\right) + 2k_1 I_4 \ddot{\varphi} \\
& + {k_1}^2 I_6 \ddot{\zeta} = 0
\end{aligned} \tag{16}
$$

2.4. Finite Element Formulations

The sandwich composite beam, which consists of multiple layers of NR-BR hybrid Magnetorheological Elastomer (MRE) with face sheets, has been modelled using elements featuring three nodes, each with five degrees of freedom (DOF), as illustrated in Figure 3. This beam element model encompasses various parameters at each node, including axial deformations of the top ($u_{1_0}^{t}$), and bottom ($u_{1_0}^{b}$) face sheets, transverse deflection (u_{3_0}), transverse rotation (φ), and higher-order term (ζ). To represent the deformation field within this distinctive element of the sandwich composite beam, we utilize nodal DOF and Lagrange interpolation functions in natural coordinates as

$$
\begin{Bmatrix} u_{1_0}^{t} \\ u_{1_0}^{b} \\ u_{3_0} \\ \varphi \\ \zeta \end{Bmatrix} = \begin{bmatrix} \widehat{N}_k & 0 & 0 & 0 & 0 \\ 0 & \widehat{N}_k & 0 & 0 & 0 \\ 0 & 0 & \widehat{N}_k & 0 & 0 \\ 0 & 0 & 0 & \widehat{N}_k & 0 \\ 0 & 0 & 0 & 0 & \widehat{N}_k \end{bmatrix} \begin{Bmatrix} u_{1_{0k}}^{t} \\ u_{1_{0k}}^{b} \\ u_{3_{0k}} \\ \varphi_k \\ \zeta_k \end{Bmatrix} \tag{17}
$$

$$
k = 1,2,3
$$

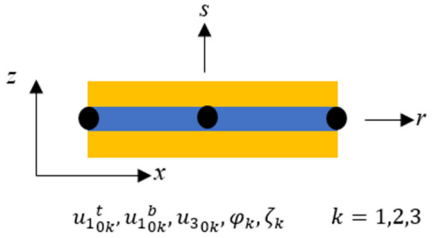

Figure 3. Three-noded beam element.

Substituting eq (14) into variational principle, and expressing in terms of finite element equation the governing equations of motion are written as

$$
[M]^{e}\{\ddot{d}\}^{e} + [K^{*}]\{d\}^{e} = \{f\}^{e} \tag{18}
$$

Preprints (www.preprints.org) | NOT PEER-REVIEWED | Posted: 20 October 2023 doi:10.20944/preprints202310.1282.v1

where $\{d\}^e$,$[M]^e$, $\{f\}^e$, and $[K^*]$ denote element deformation vector, element mass matrix, element force vector and element stiffness matrix respectively. After the assembly of element mass matrix and stiffness matrix, the governing equations of motion for composite beam is given as

$$[M]\{\ddot{q}\} + [K^*]\{q\} = \{f\} \tag{19}$$

$\{d\}$, $[M]$, $\{f\}$, and $[K^*]$ denote global deformation vector, mass matrix, force vector, and global complex stiffness matrix respectively. The force vector for free vibration is considered to be null thereby reducing the eq (17) as

$$[M]\{q\} + [K^*]\{q\} = \{0\} \tag{20}$$

The solution $\{d\}$ for the eq. (19) can be expressed in terms of arbitrary constant (C_1) as

$$\{q\} = [C_1]\{e^{\lambda t}\} \tag{21}$$

Eq. (21) reduces the eq. (20) into eigen value problem as

$$\left[[M] - \lambda[K^*]\right]\{C_1\} = 0 \tag{22}$$

where λ is the characteristic value which is obtained as

$$\lambda = \left[\because \lambda_j \because\right] \tag{23}$$

The physical deformation vector can be determined using eq. (21) only after formulating the deformation vector $q(t)$ from the eq. (20).

The natural frequency (ω_j) and loss factor (η_j) at each mode are obtained using the eq. (23) as

$$\omega_j = \sqrt{Re(\lambda_j)}$$
$$\eta_j = \frac{Im(\lambda_j)}{Re(\lambda_j)} \tag{24}$$

2.5. Validation of Established Finite Element Formulation

The validity of Finite element simulations is verified by comparing the natural frequencies of MR fluid sandwich beam with elastic face layers obtained from the available literature using developed MATLAB code. The geometrical and mechanical properties of sandwich composite are considered to be same as that of Rajmohan et al. [30]. Elastic layer length = 300 mm, breadth b= 30 mm, thickness h_e= 1 mm, elastic modulus E_e =68GPa, storage modulus G_e=26 GPa, density of elastic layer ϱ_e = 2700 kg/m3, MR fluid core thickness h_c= 1 mm, density of rubber ϱ_r = 1233 kg/m3, density of MR fluid ϱ_{cf} = 3500 kg/m3, shear modulus function of MR fluid G'= -3.3691G^2+4.9975 x 10^3G + 0.893 MPa, G''= 0.9 G^2+0.8124 x 10^3G+0.1855 MPa where G indicates the applied magnetic field intensity in Gauss. The simulations are performed to obtain first five natural frequencies of three-layer MR fluid sandwich composite at 0 G and 250 G magnetic field under simply supported boundary condition. The simulated natural frequencies are correlated with that of Rajmohan et al. [30] and Rajmohan et al. [31] as presented in the Table 2. The maximum deviation observed between the simulated frequencies with the frequencies presented by Rajmohan et al. [30] is 8% and with that of Rajmohan et al. [31] is 4%. The models used in Rajmohan et al. [30] and Rajmohan et al. [31] assume no warping of transverse normal during the deformation resulting in the deviations of the results. Therefore, the developed FE model based on Reddy third order shear deformation can be considered to be a better model in evaluating the dynamic characteristics of sandwich composite beam. Further, conclusion may be drawn, that the proposed model has good agreement with Rajmohan et al. [30] and Rajmohan et al. [31] in predicting the natural frequencies of three-layer MR fluid composite beam.

In addition to using finite element simulations for predicting and comprehending the dynamic behaviour of MR elastomer sandwich composite structures, the validation of the FEM approach is further substantiated by comparing the loss factor with data obtained by RajaMohan et al. [31] for MRE sandwich composite structures. This comprehensive validation underscores the accuracy of the finite element model in capturing intricate interactions and behaviours within such composite structures. By achieving strong alignment with prior research, the model instils confidence in its capability to predict and analyze the dynamic responses of similar MR elastomer sandwich composite structures.

Preprints (www.preprints.org) | NOT PEER-REVIEWED | Posted: 20 October 2023 doi:10.20944/preprints202310.1282.v1

Table 2. Comparison of natural frequencies of sandwich beam determined from present FEM with that reported in [30,31].

Magnetic field in Gauss	Modes	Natural Frequencies (Hz)				
		Present FEM	Ref [30]	Ref [31]	Error % [30]	Error % [31]
0	1	38.84	40.34	40.74	3.71839	4.66372
	2	105.45	103.1	105.7	2.27934	0.23652
	3	210.93	200.07	206.51	5.4281	2.14033
	4	356.45	332.45	344.72	7.21913	3.40276
	5	542.6	501.67	521.57	8.15875	4.03206
250	1	51.57	50.92	51.88	1.27651	0.59753
	2	125.2	120.32	123.56	4.05585	1.32729
	3	235.47	222.24	229.01	5.95302	2.82084
	4	383.33	357.33	369.67	7.27619	3.69519
	5	570.92	528.15	547.94	8.09808	4.19389

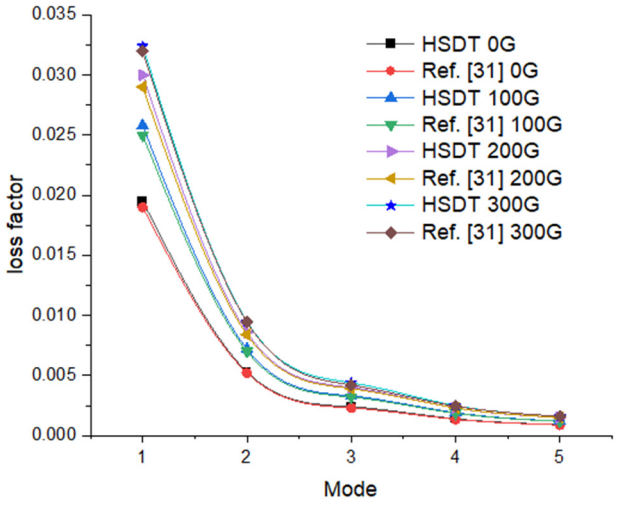

Figure 4. Variation of loss factor of five modes under various magnetic field.

3. Results

Finite element simulations are performed on hybrid MRE sandwich composite beam having dimensions 300 mm × 30 mm × 4 mm to evaluate loss factor and natural frequencies. The face sheet is assumed to be three-layer fibre reinforced polymer laminate with the layup sequence of $[0^{\circ}/90^{\circ}/0^{\circ}]_s$ having 0.54 mm thickness. The hybrid elastomer thickness is considered to be 3 mm. The mechanical properties of face sheet [32]and rheological properties of hybrid elastomer [26] considered for the simulation are given in Table 3 and Table 4 respectively. Analysis was performed under varying magnetic field intensity from 0mT to 750mT and three different end conditions namely both ends clamped (CC), one end clamped and free at another end (CF) and simply supported at both ends (SS). The damping characteristics and natural frequencies of sandwich composite beam are highly influenced by matrix mixture (NR/PBR) content, magnetic field intensity, Ply orientation, thickness ratio and boundary conditions. The change in loss factor has a substantial effect on damping properties of composite beam. Therefore, it is essential to examine the influence of all these parameters on dynamic properties of sandwich composite beam.

Preprints (www.preprints.org) | NOT PEER-REVIEWED | Posted: 20 October 2023 doi:10.20944/preprints202310.1282.v1

Table 3. Rheological properties of hybrid MRE samples under various magnetic field.

Rheological properties	Magnetic field in mT	Hybrid MRE			
		SC1	SC2	SC3	SC4
G′(MPa)	0	0.48	0.45	0.43	0.4
	150	0.53	0.51	0.49	0.45
	300	0.6	0.595	0.56	0.53
	450	0.63	0.625	0.6	0.57
	600	0.635	0.615	0.62	0.59
	750	0.62	0.61	0.615	0.6
η	0	0.104	0.118	0.128	0.15
	150	0.1	0.11	0.118	0.144
	300	0.08	0.09	0.108	0.134
	450	0.07	0.08	0.104	0.128
	600	0.065	0.08	0.102	0.128
	750	0.064	0.078	0.102	0.124

Table 4. Properties of fiber lamina and density of MRE core of various samples.

Lamina properties	Density of MRE samples
E_1 = 30.5GPa	
E_2 = 6.99Gpa	ρ_{SC1} = 2135.569 kg/m^3
ν_{12}= 0.269	ρ_{SC2} = 2119.201 kg/m^3
G_{12} = 2.8Gpa	ρ_{SC3} = 2103.081 kg/m^3
$G_{13} = G_{12}$	ρ_{SC4} = 2063.836 kg/m^3
G_{23} = 2.51Gpa	
ρ= 1745 kg/m^3	

3.1. Influence of applied magnetic field intensity on natural frequency and loss factor of sandwich composite beam

The investigation is conducted to examine the effect of applied magnetic field intensity on natural frequencies and loss factor of sandwich composite beam. The extracted fundamental natural frequencies of sandwich composite beams with various hybrid elastomer cores such as SC1, SC2, SC3 and SC4 are plotted for various magnetic field and boundary conditions as shown in Figure 5. It can be clearly seen from Figure 5 that at zero magnetic field the fundamental natural frequency increases by 3% under CF, 2% under CC and 4% under SS boundary conditions respectively, with increase in NR content from 0 to 90phr. The increment in natural frequencies of all the configurations could be due to improvement in stiffness of hybrid MR elastomer resulting from increased strain crystallization with the increase in NR content [26]. The maximum increase in the fundamental natural frequency of SC1, SC2, SC3 and SC4 based composite beams is found to be 7.6%, 8.5%, 10.1% 10.4% respectively at 600mT under CF boundary condition. The highest improvement in fundamental natural frequency is observed in SC4 based composite beam. This can be due to increased compatibility of CI particles with PBR which restricts the motion of rubber molecules resulting in improved field dependent modulus. Further, the first five natural frequencies of various sandwich composite beams for various magnetic field and boundary conditions are presented in Table 5. It can be seen that with applied magnetic field intensity the natural frequencies at all the modes tend to increase up-to 600mT and further it is observed that there is slight decrement at higher intensity of magnetic field. The cause of this decrement at higher magnetic strength can be ascribed to agglomeration of magnetic filler particles and breakdown of separated filler chains [33]. Also, the results indicate that CC and CF boundary conditions have highest and least natural frequencies respectively under all intensities of magnetic field. This can be attributed to the fact that the clamped ends provide higher stiffness to the beam when compared to free end.

Preprints (www.preprints.org) | NOT PEER-REVIEWED | Posted: 20 October 2023 doi:10.20944/preprints202310.1282.v1

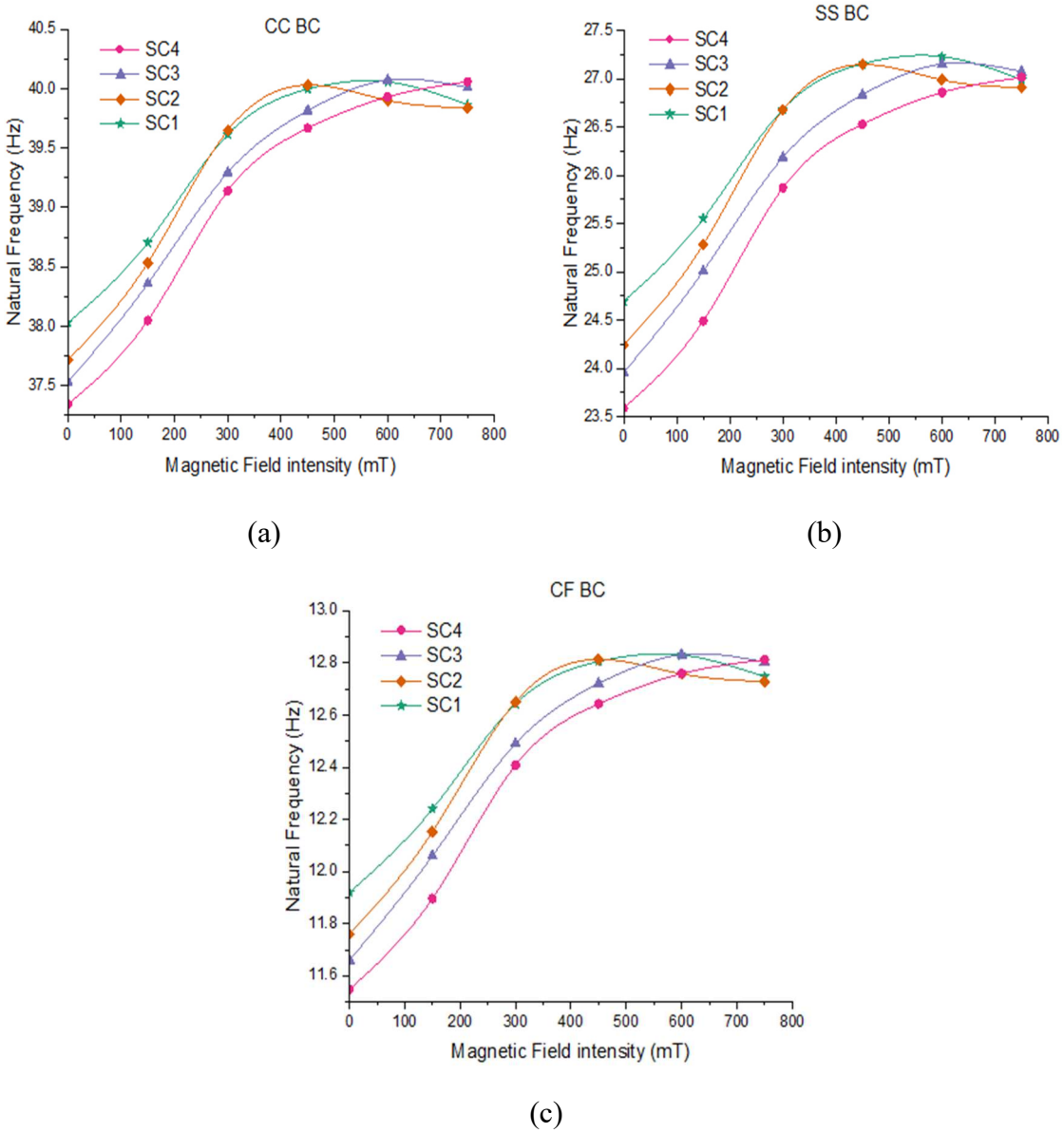

Figure 5. Influence of intensity of magnetic field on natural frequencies of sandwich beam under (a) CC boundary condition; (b) SS boundary condition; (c) CF boundary condition.

The loss factor at fundamental mode of various sandwich composite beams is plotted for various boundary conditions with intensity of magnetic field as shown in Figure 6. Referring to Figure 6, the improvement in loss factor increases from 66% to 136% with increase in magnetic field intensity from 0 to 600mT when PBR content increases from 10% to 100% under CF boundary condition. This increase in damping can be due to increased interfacial friction between hybrid matrix and CI particles resulting from intermolecular interaction as the PBR content is increased. Further, loss factor for SC1, SC2, SC3 and SC4 based composite beams is found to decrease by 54%, 50%, 44% and 43% respectively when magnetic field increases from 0mT to 600mT for CF boundary condition. Under the externally applied magnetic field the alignment of CI particles restricts the movement of hybrid rubber matrix molecules resulting in reduced energy dissipation thereby reducing the loss factor [34]. It can be observed that SS and CC boundary conditions have largest and lowest loss factor respectively under all magnetic field intensity.

Preprints (www.preprints.org) | NOT PEER-REVIEWED | Posted: 20 October 2023 doi:10.20944/preprints202310.1282.v1

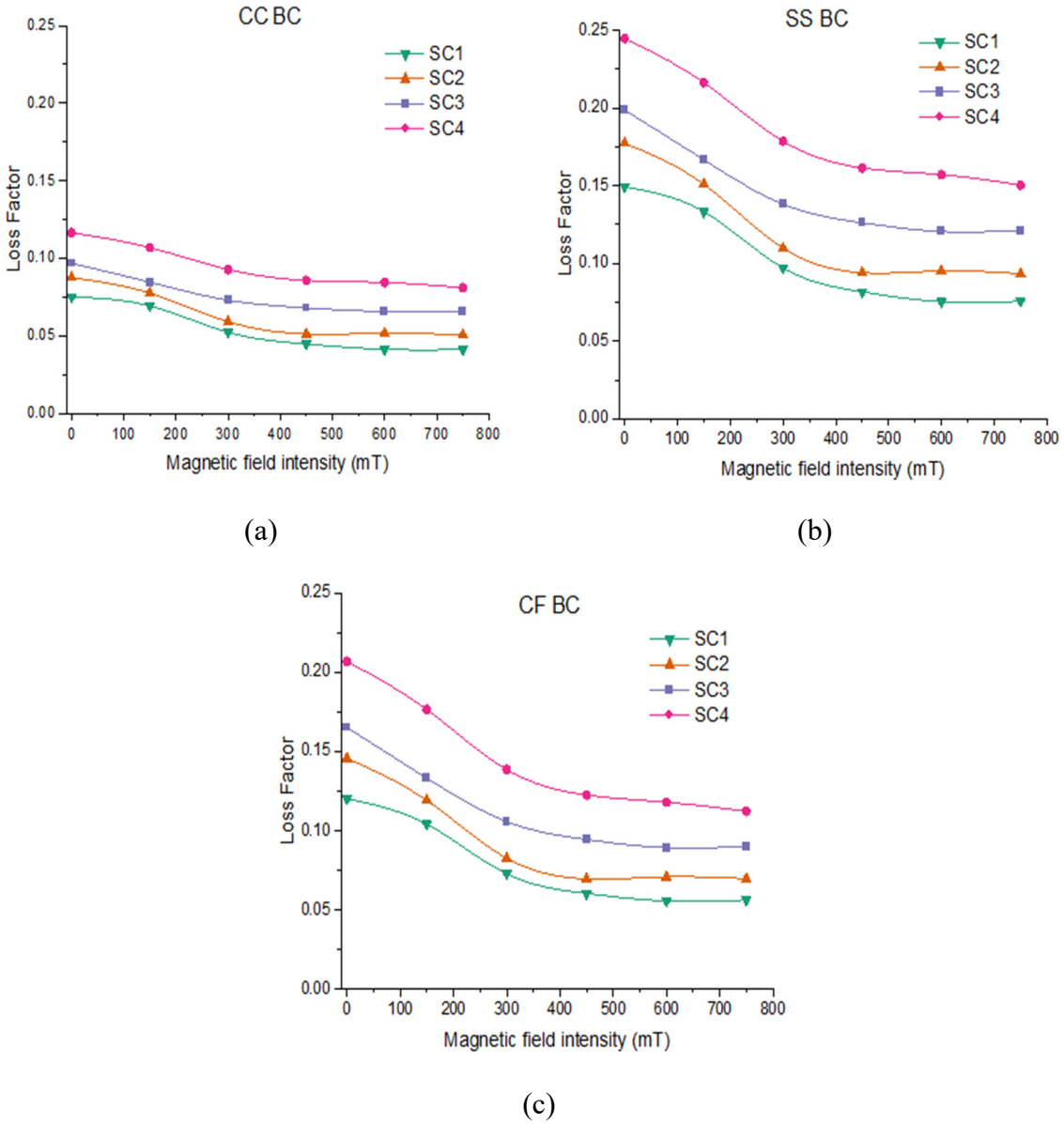

Figure 6. Influence of intensity of magnetic field on Loss factor of sandwich beam under (a) CC boundary condition; (b) SS boundary condition; (c) CF boundary condition.

Table 5. First five natural frequencies (Hz) of samples under various boundary conditions.

MRE Samples	BC	Modes	Magnetic field intensity					
			0mT	150mT	300mT	450mT	600mT	750mT
SC1	CF	1	11.91927	12.23997	12.64273	12.80502	12.82992	12.74658
		2	45.01107	46.00776	47.30127	47.83229	47.91597	47.64571
		3	101.103	102.6293	104.6851	105.5459	105.6853	105.2511
		4	181.2576	182.9202	185.1959	186.1578	186.3154	185.832
		5	287.6339	289.3705	291.7678	292.7863	292.9542	292.4434
	CC	1	38.03013	38.70405	39.61301	39.99392	40.05566	39.8636
		2	94.71789	95.76178	97.18789	97.79	97.88851	97.58583
		3	176.3394	177.5886	179.3127	180.0451	180.1658	179.7985
		4	283.5065	284.8658	286.7509	287.5541	287.687	287.2846
		5	416.3424	417.772	419.7603	420.6089	420.7497	420.3247
	SS	1	24.69532	25.54928	26.68158	27.15184	27.22716	26.98907

Preprints (www.preprints.org) | NOT PEER-REVIEWED | Posted: 20 October 2023 doi:10.20944/preprints202310.1282.v1

		2	67.63693	68.88882	70.58256	71.29368	71.4092	71.05091
		3	135.555	137.0116	139.0114	139.8581	139.9972	139.572
		4	229.2759	230.8229	232.962	233.8717	234.0219	233.5658
		5	348.9798	350.5754	352.7908	353.7352	353.8916	353.4186
		1	11.75898	12.15231	12.65093	12.81342	12.75771	12.72833
		2	44.52597	45.74274	47.33647	47.86851	47.68779	47.59405
	CF	3	100.4284	102.28	104.7992	105.6623	105.3719	105.2239
		4	180.6903	182.7003	185.4814	186.4458	186.1226	185.9592
		5	287.2749	289.3705	292.2959	293.3171	292.9755	292.8036
		1	37.71648	38.53371	39.64736	40.02929	39.90083	39.83541
		2	94.31609	95.57862	97.32214	97.92584	97.72343	97.62098
SC2	CC	3	176.0078	177.5151	179.6192	180.3535	180.1079	179.9842
		4	283.3637	285.0022	287.3008	288.106	287.837	287.7019
		5	416.4742	418.1965	420.6196	421.4703	421.1863	421.0438
		1	24.24428	25.28294	26.6736	27.14497	26.98575	26.904
		2	67.04697	68.56414	70.63811	71.35109	71.11147	70.98963
	SS	3	135.0022	136.762	139.2047	140.0537	139.7694	139.6258
		4	228.8914	230.7574	233.367	234.2791	233.9742	233.8208
		5	348.8513	350.7743	353.475	354.4219	354.1056	353.9468
		1	11.65949	12.05975	12.48997	12.72023	12.83099	12.80317
		2	44.23157	45.46578	46.82328	47.56404	47.92454	47.83414
	CF	3	100.0493	101.918	104.0327	105.2122	105.7935	105.648
		4	180.4456	182.4686	184.7872	186.0933	186.7409	186.5789
		5	287.2523	289.3583	291.7882	293.1644	293.8489	293.6777
		1	37.53344	38.35807	39.29232	39.81385	40.07105	40.00666
		2	94.11703	95.38822	96.84298	97.66154	98.06707	97.9656
SC3	CC	3	175.9186	177.4335	179.1813	180.1711	180.6634	180.5402
		4	283.4835	285.1288	287.0342	288.1165	288.6557	288.5208
		5	416.8804	418.6089	420.615	421.7565	422.3259	422.1835
		1	23.95817	25.00864	26.18315	26.83226	27.15054	27.0708
		2	66.70005	68.23012	69.96768	70.93952	71.41935	71.29923
	SS	3	134.7329	136.5032	138.537	139.6849	140.2546	140.1121
		4	228.8072	230.6819	232.8479	234.076	234.6872	234.5343
		5	349.0311	350.9617	353.1993	354.4711	355.1051	354.9465
		1	11.54746	11.89634	12.40732	12.6425	12.75894	12.81197
		2	43.90747	44.97459	46.57497	47.32921	47.70346	47.87907
	CF	3	99.71048	101.3052	103.7732	104.9695	105.5649	105.8531
		4	180.485	182.1989	184.8887	186.2093	186.8678	187.1909
		5	287.8643	289.6414	292.451	293.84	294.5333	294.8759
		1	37.3451	38.04833	39.1381	39.66698	39.93023	40.0578
		2	94.03016	95.10808	96.79713	97.6252	98.03797	98.24016
SC4	CC	3	176.1791	177.4576	179.4787	180.4778	180.9764	181.2228
		4	284.3001	285.6855	287.8844	288.9756	289.5205	289.7908
		5	418.4291	419.8824	422.1949	423.345	423.9196	424.2053
		1	23.59108	24.4924	25.86879	26.52818	26.85595	27.01257
		2	66.33237	67.63541	69.65979	70.64462	71.13501	71.37328
	SS	3	134.6308	136.1285	138.4853	139.6453	140.2239	140.5084
		4	229.194	230.7747	233.2775	234.5165	235.135	235.4411
		5	350.0858	351.7104	354.2917	355.5737	356.214	356.5319

Preprints (www.preprints.org) | NOT PEER-REVIEWED | Posted: 20 October 2023 doi:10.20944/preprints202310.1282.v1

3.2. Influence of MRE core thickness on natural frequencies and loss factor of sandwich composite beam

The effect of the MRE core thickness on the fundamental loss factor and natural frequency of sandwich composite beams is summarized in Table 6 and 7. It is evident that as the core thickness increases from 1.5mm to 4.5mm, the fundamental natural frequency of composite beams for SC1, SC2, SC3, and SC4 increases by approximately 16%, 15.5%, 14.8%, and 14.2%, respectively, under zero magnetic field conditions with clamped-free (CF) boundary conditions. This increase in natural frequency can be attributed to the greater stiffness of the beam resulting from the thicker core. Furthermore, Table 7 reveals that the loss factor for composite beams SC1, SC2, SC3, and SC4 increases by 75%, 78%, 80%, and 84%, respectively, at zero magnetic field under CF boundary conditions. This significant improvement in damping properties is likely due to the increased interfacial friction between the hybrid matrix and CI particles within the thicker core. These findings underscore the potential for optimizing the mechanical and damping properties of sandwich composite beams by carefully selecting and adjusting the thickness of the MRE core, offering valuable insights for engineering applications requiring vibration control and damping.

Table 6. Variation of fundamental natural frequency (Hz) of MRE samples with core thickness.

MRE samples	Core Thickness in mm	Magnetic field intensity					
		0mT	150mT	300mT	450mT	600mT	750mT
SC1	1.5	10.6914	10.8794	11.10873	11.19967	11.21329	11.16621
	3	11.91927	12.23997	12.64273	12.80502	12.82992	12.74658
	4.5	12.44153	12.83503	13.33595	13.53934	13.5709	13.46684
SC2	1.5	10.60031	10.83163	11.11646	11.20739	11.17595	11.15912
	3	11.75898	12.15231	12.65093	12.81342	12.75771	12.72833
	4.5	12.2431	12.72488	13.34401	13.5478	13.4782	13.44174
SC3	1.5	10.5446	10.78049	11.02885	11.15951	11.22172	11.20608
	3	11.65949	12.05975	12.48997	12.72023	12.83099	12.80317
	4.5	12.11953	12.6092	13.14075	13.42756	13.56618	13.53139
SC4	1.5	10.48757	10.69432	10.99049	11.12393	11.1899	11.21911
	3	11.54746	11.89634	12.40732	12.6425	12.75894	12.81197
	4.5	11.97644	12.40191	13.0317	13.32452	13.46963	13.53654

Table 7. Variation of loss factor of MRE samples with core thickness.

MRE samples	Core Thickness in mm	Magnetic field intensity					
		0mT	150mT	300mT	450mT	600mT	750mT
SC1	1.5	0.080276	0.068653	0.047367	0.039047	0.035921	0.036456
	3	0.12041	0.10418	0.07294	0.0605	0.05571	0.05635
	4.5	0.140402	0.122066	0.085988	0.071504	0.065862	0.066524
SC2	1.5	0.097727	0.078866	0.053746	0.045009	0.045928	0.045254
	3	0.145748	0.119227	0.082726	0.069694	0.070963	0.069839
	4.5	0.169567	0.139482	0.097502	0.082351	0.083772	0.0824
SC3	1.5	0.111208	0.088485	0.069208	0.061286	0.057731	0.058316
	3	0.165264	0.133245	0.105829	0.094524	0.089416	0.090226
	4.5	0.192022	0.15564	0.1244	0.111516	0.105678	0.106586
SC4	1.5	0.139705	0.117939	0.091056	0.079836	0.076545	0.072718
	3	0.206857	0.176515	0.138642	0.122572	0.118034	0.112333
	4.5	0.240098	0.205741	0.162717	0.144349	0.139262	0.132634

a

Preprints (www.preprints.org) | NOT PEER-REVIEWED | Posted: 20 October 2023 doi:10.20944/preprints202310.1282.v1

3.3. Influence of ply orientation natural frequency and on loss factor of sandwich composite beam

The study focuses on the damping characteristics and natural frequency of sandwich composite beam samples with three different ply orientations: [0°/90°/0°]s, [90°/0°/90°]s, and [0°/90°/45°]s, and their respective effects are summarized in Tables 8 and 9. It is noteworthy that the fundamental natural frequency of all beam configurations at zero magnetic field, under clamped-free (CF) boundary conditions, follows the order of ply orientation: $[90°/0°/90°]_s$, $[0°/90°/45°]_s$, and $[0°/90°/0°]_s$. Specifically, the natural frequency increases by 11% for $[0°/90°/0°]_s$ and 10% for $[0°/90°/45°]_s$ compared to $[90°/0°/90°]_s$ across all composite beam configurations. The lowest natural frequency is associated with the ply orientation $[90°/0°/90°]_s$, signifying that the outermost face-sheet with a 90° orientation contributes to decreased beam stiffness. Furthermore, under zero magnetic field and CF boundary conditions, the loss factor for all beam configurations follows the order of ply orientation: $[90°/0°/90°]_s$, $[0°/90°/0°]_s$, and $[0°/90°/45°]_s$. Notably, the loss factor increases by 1% for $[0°/90°/0°]_s$ and 15% for $[0°/90°/45°]_s$ compared to $[90°/0°/90°]_s$ across all composite beam configurations. While $[0°/90°/45°]_s$ exhibits a high loss factor, the natural frequency remains relatively lower due to the 45° ply introducing shear forces, which reduce beam stiffness. The increase in the loss factor can be attributed to heightened energy dissipation facilitated by the unrestricted motion of rubber molecules caused by the presence of carbonyl iron (CI) particles in the hybrid matrix. These results collectively demonstrate the intricate interplay between ply orientation, natural frequency, and loss factor, shedding light on the dynamic behavior of the sandwich composite beams.

Table 8. Effect of ply orientation on fundamental natural frequency of sandwich composite beam.

Magnetic field intensity mT	[0°/90°/0°]s				[90°/0°/90°]s				[0°/90°/45°]s			
	SC1	SC2	SC3	SC4	SC1	SC2	SC3	SC4	SC1	SC2	SC3	SC4
0	11.919	11.758	11.659	11.547	10.640	10.501	10.415	10.321	11.766	11.582	11.467	11.335
150	12.239	12.152	12.059	11.896	10.919	10.844	10.765	10.627	12.134	12.035	11.925	11.734
300	12.642	12.650	12.489	12.407	11.265	11.274	11.138	11.071	12.598	12.607	12.420	12.322
450	12.805	12.813	12.720	12.642	11.404	11.412	11.336	11.274	12.786	12.795	12.686	12.594
600	12.829	12.757	12.830	12.758	11.425	11.365	11.430	11.374	12.815	12.730	12.814	12.728
750	12.746	12.728	12.803	12.811	11.353	11.339	11.406	11.419	12.718	12.696	12.781	12.790

Table 9. Effect of ply orientation on loss factor of sandwich composite beam.

Magnetic field intensity mT	[0°/90°/0°]s				[90°/0°/90°]s				[0°/90°/45°]s			
	SC1	SC2	SC3	SC4	SC1	SC2	SC3	SC4	SC1	SC2	SC3	SC4
0	0.1204	0.1457	0.1652	0.2068	0.1184	0.1439	0.1637	0.2057	0.1392	0.1685	0.1912	0.2396
150	0.1041	0.1192	0.1332	0.1765	0.1016	0.1166	0.1307	0.1741	0.1204	0.1378	0.1541	0.2043
300	0.0729	0.0827	0.1058	0.1386	0.0703	0.0798	0.1027	0.1350	0.0843	0.0956	0.1224	0.1604
450	0.0605	0.0696	0.0945	0.1225	0.0581	0.0670	0.0911	0.1186	0.0699	0.0806	0.1093	0.1418
600	0.0557	0.0709	0.0894	0.1180	0.0534	0.0683	0.0859	0.1139	0.0644	0.0820	0.1034	0.1366
750	0.0563	0.0698	0.0902	0.1123	0.0542	0.0673	0.0868	0.1082	0.0651	0.0807	0.1043	0.1300

3.4. Frequency response of hybrid MRE sandwich composite beam

The investigation focused on the transverse vibration response of the hybrid MRE sandwich composite beam (SC1) under the constraint-free (CF) boundary condition, with varying magnetic field intensities. The responses were analyzed across a frequency range of 1-250 Hz by considering harmonic excitation force of magnitude 5 N at free end corner of the beam. Forced vibration simulation is performed on various, as depicted in Figure 7. In Figure 7, it is evident that there is a noticeable leftward shift in the natural frequency as the magnetic field intensity increases. This

Preprints (www.preprints.org) | NOT PEER-REVIEWED | Posted: 20 October 2023 doi:10.20944/preprints202310.1282.v1

phenomenon can be attributed to appreciation in the stiffness with the rise in magnetic field strength. Additionally, it can be observed that the amplitude of vibration decreases with higher magnetic field intensities. Figure 8 presents the vibration responses of all configurations of composite beams at 450 mT. Due to variations in the stiffness of the beams, slight fluctuations in responses at certain modes can be observed. These results imply that the application of a magnetic field has a significant impact on the transverse vibration behavior of the hybrid MRE sandwich composite beam. As the magnetic field intensity increases, the natural frequencies shift to higher values, and the amplitudes of vibration decrease. This finding suggests the potential for precise control and tuning of the dynamic response of such composite structures, which is promising for various engineering applications where vibration control and damping are crucial.

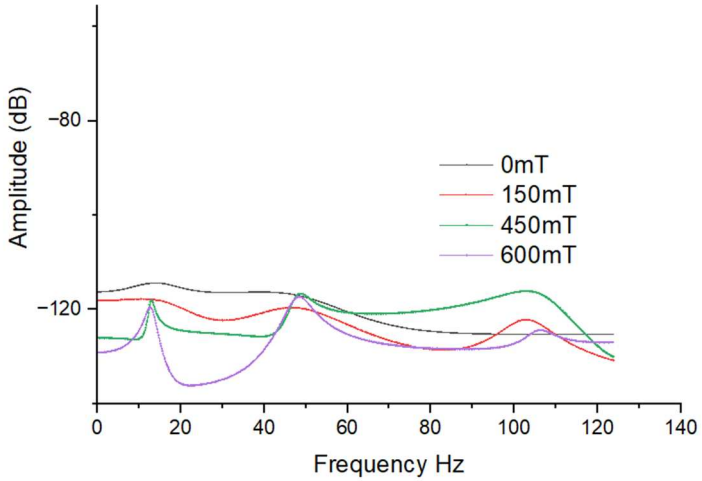

Figure 7. Transverse vibration response of hybrid MRE sandwich composite beam (SC1) under CF boundary condition.

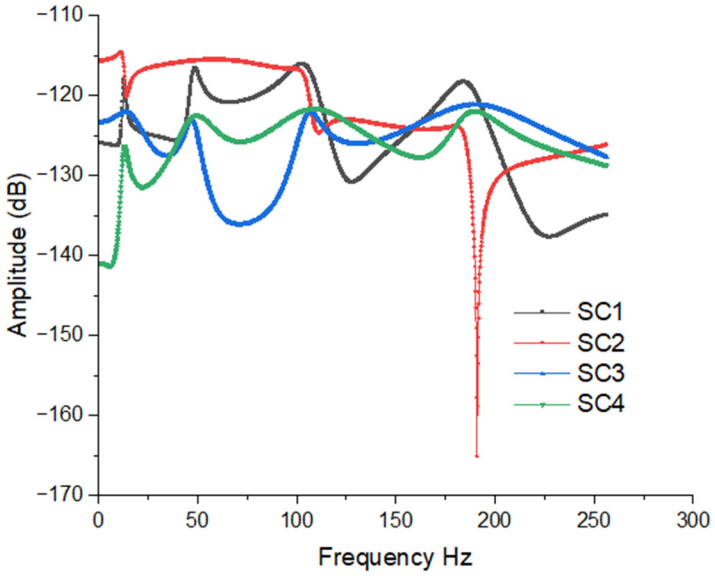

Figure 8. FRF plot of all configurations of hybrid MRE sandwich composite beam.

4. Conclusions

The paper extensively investigates the dynamic characteristics of MR hybrid sandwich composite beams with various configurations. It utilizes differential equations based on the Reddy third-order shear deformation theory (RTSDT) to gain valuable insights into behavior of the structures. The study emphasizes the significant impact of magnetic field intensity and the ratio of

Preprints (www.preprints.org) | NOT PEER-REVIEWED | Posted: 20 October 2023 doi:10.20944/preprints202310.1282.v1

PBR to NR on the natural frequency and loss factor of hybrid MR elastomer sandwich composite beams. Additionally, an exploration of factors such as ply orientation, boundary conditions, and elastomer core thickness provides a comprehensive understanding of these variables affecting the dynamic properties of the sandwich composite structure. The study observes that natural frequencies increase with magnetic field intensity up to 600 mT but decrease beyond that due to filler chain breakdown and particle agglomeration. Furthermore, an increase in PBR content notably improves damping properties, as evidenced by a significant increase in the loss factor. Similarly, an increase in NR content enhances stiffness, as seen in the rise of the fundamental natural frequency. Ply orientation is found to impact natural frequencies, with a significant 11% increase observed for the [0°/90°/0°]s orientation. Finally, an increase in elastomer core thickness contributes to higher natural frequencies and improved damping. This research provides practical guidance for engineering applications, enabling the optimization of hybrid MR elastomer sandwich composite beams for various structural purposes. By tailoring factors such as magnetic field intensity, composition, and structural configurations, these materials can effectively enhance the performance, safety, and longevity of various structural systems and equipment.

Author Contributions: Conceptualization, Lakshmi Pathi J; Data curation, Mohanraj T; Formal analysis, Ahobal N and Lakshmi Pathi J; Investigation, Ahobal N and Lakshmi Pathi J; Project administration, Sakthivel G and Yogesh Bhalerao; Resources, Mohanraj T; Software, Jegadeeshwaran R; Supervision, Sakthivel G and Yogesh Bhalerao; Validation, Jegadeeshwaran R; Writing – original draft, Lakshmi Pathi J; Writing – review & editing, Jegadeeshwaran R.

Funding: The authors declare no funding details.

Data Availability: The data used to support the findings of this study are included within the article.

Acknowledgments: The authors thank the Management of Vellore Institute of Technology, VIT Chennai and Amrita School of Engineering, Coimbatore, Amrita Vishwa Vidyapeetham, India, and for their support to publish this work.

Conflicts of Interest: "The authors declared no conflict of interest".

Appendix-I

From equation 6 we have $\{N^j\} = [ABD]\{\varepsilon^j\}$

where, $\{N^j\} = \begin{Bmatrix} N^j \\ M^j \\ P^j \\ Q^j \\ R^j \end{Bmatrix}$, $[ABD] = \begin{bmatrix} A & B & E & 0 & 0 \\ B & D & F & 0 & 0 \\ E & F & H & 0 & 0 \\ 0 & 0 & 0 & A_s & D_s \\ 0 & 0 & 0 & D_s & F_s \end{bmatrix}$, $\{\varepsilon^j\} = \begin{Bmatrix} \varepsilon_0^j \\ \varepsilon_1^j \\ \varepsilon_3^j \\ \gamma_0^j \\ \gamma_2^j \end{Bmatrix}$

Therefore, $\{N^j\} = [ABD]\{\varepsilon^j\}$ is given as

$$\begin{Bmatrix} N^j \\ M^j \\ P^j \\ Q^j \\ R^j \end{Bmatrix} = \begin{bmatrix} A & B & E & 0 & 0 \\ B & D & F & 0 & 0 \\ E & F & H & 0 & 0 \\ 0 & 0 & 0 & A_s & D_s \\ 0 & 0 & 0 & D_s & F_s \end{bmatrix} \begin{Bmatrix} \varepsilon_0^j \\ \varepsilon_1^j \\ \varepsilon_3^j \\ \gamma_0^j \\ \gamma_2^j \end{Bmatrix} \quad \text{(i)}$$

$$(I_0, I_1, I_2, I_3, I_4, I_6) = \sum_{j=1}^{n} \int_{h_j}^{h_{j+1}} \rho(1, x_3, {x_3}^2, {x_3}^3, {x_3}^4, {x_3}^6) dx_3 \quad \text{(ii)}$$

References

1. Bica, I.; Liu, Y. D.; and Choi, H. J. Physical characteristics of magnetorheological suspensions and their applications. *J. Ind Eng Chem.* 2013, 19, 394–406.
2. Ashtiani, M.; Hashemabadi, S.; and Ghaffari, A. A review on the magnetorheological fluid preparation and stabilization. *J. Magn. Magn Mater.* 2015, 374, 716–730.

3. Carlson, J. D.; and Jolly, M. R. MR fluid, foam and elastomer devices. *Mechatronics.* 2000, 10, 555–569.
4. Jolly M. R.; Carlson J. D.; and Munoz B. C. A model of the behavior of magnetorheological materials. *Smart Mater. Struct*. 1996, 5, 607.
5. Khimi, S. R.; and Pickering, K. The effect of silane coupling agent on the dynamic mechanical properties of iron sand/natural rubber magnetorheological elastomers. *Compos. B. Eng.* 2016, 90, 115–125.
6. Park, B. O.; Park, B. J.; Hato, M. J.; and Choi, H. J. Soft magnetic carbonyl iron microsphere dispersed in grease and its rheological characteristics under magnetic field. *Colloid Polym. Sci.* 2011, 289, 381–386.
7. Guo, F.; Du, C.-b; and Li, R.-p. Viscoelastic parameter model of magnetorheological elastomers based on Abel dashpot. *Adv. Mech. Eng.* 2014, 6, 629386.
8. Deng, H.-X.; and Gong, X.-l. Application of magnetorheological elastomer to vibration absorber. *Commun Nonlinear Sci Numer Simul.* 2008, 13, 1938–1947.
9. Chen, L; Gong, X. L.; and Li, W. H. Damping of magnetorheological elastomers. *Chinese J. Chem. Phys*. 2008, 6, 581-5.
10. Boczkowska, A.; Awietjan S. F.; Pietrzko. S.; and Kurzydłowski K. J. Mechanical properties of magnetorheological elastomers under shear deformation. *Compos. B. Eng.* 2012, 2, 636-40.
11. Deng, H. X.; Gong, X. L.; and Wang, L. H. Development of an adaptive tuned vibration absorber with magnetorheological elastomer. *Smart Mater. Struct*. 2006, 5, N111.
12. Jung, H. S.; Kwon, S. H.; Choi, H. J.; Jung, J. H.; and Kim Y. G. Magnetic carbonyl iron/natural rubber composite elastomer and its magnetorheology. *Compos Struct.* 2016, 136, 106–112.
13. Gong, X.; Zhang, X.; and Zhang, P. Fabrication and characterization of isotropic magnetorheological elastomers. *Polym. Test.* 2005, 24, 669–676.
14. Chen, L.; Gong, X.-l.; Jiang, W.-q.; Yao, J.-j.; Deng, H.-x.; and Li, W.-h. Investigation on magnetorheological elastomers based on natural rubber. *J. Mater. Sci.* 2007, 42, 5483–5489.
15. Hafeez, A. M.; Usman, M.; Umer, M. A.; and Hanif, A.; Recent Progress in Isotropic Magnetorheological Elastomers and Their Properties: A Review. *Polymers*, 2020, 12, 3023-34.
16. Fan, Y.C.; Gong, X.L.; Jiang, W.Q.; Zhang, W.; Wei, B.; Li, W.H. Effect of maleic anhydride on the damping property of magnetorheological elastomers, *Smart Mater. Struct.* 2010, 19, 055015.
17. Burgaz, E.; and Goksuzoglu, M. Effects of magnetic particles and carbon black on structure and properties of magnetorheological elastomers, *Polym. Test*. 2020, 81, 106233-12.
18. Pickering, K.L.; Khimi, S. R.; Ilanko, S. The effect of silane coupling agent on iron sand for use in magnetorheological elastomers Part 1: surface chemical modification and characterization, *Compos A Appl.* 2015, 68, 377–386.
19. Poojary, U.R.; Hegde, S.; and Gangadharan, K.V. Experimental investigation on the effect of carbon nanotube additive on the field-induced viscoelastic properties of magnetorheological elastomer, *J. Mater. Sci.* 2018, 53, 4229–4241.
20. Khimi, S.R.; and Pickering, K.L. The effect of silane coupling agent on the dynamic mechanical properties of iron sand/natural rubber magnetorheological elastomers, *Compos. B Eng.* 2016, 90, 115–125.
21. Bokobza, L. Elastomer Nanocomposites: Effect of Filler–Matrix and Filler–Filler Interactions. *Polymers* 2023, 15, 2900-22.
22. Zaman, I.; Manshoor, B.; Khalid, A.; and Araby, S. From clay to graphene for polymer nanocomposites—a survey. *J Polym Res.* 2014, 21, 429-11.
23. Jovanović, S.; Samaržija-Jovanović, S.; Marković, G.; Jovanović,V.; Adamović, T.; Marinović-Cincović, M. Ternary NR/BR/SBR rubber blend nanocomposites. *J. Thermoplast. Compos. Mater.* 2018, 31, 265-287. doi:10.1177/0892705717697778.
24. Abdelsalam A, Araby S, El-Sabbagh S, et al. Effect of carbon black loading on mechanical and rheological properties of natural rubber/styrene-butadiene rubber/nitrile butadiene rubber blends. J Thermoplast Compos. DOI: 10.1177089270571984455 6
25. Zhang, W.; Gong, X.; Xuan, S.; Jiang, W. Temperature-dependent mechanical properties and model of magnetorheological elastomers. *Ind Eng Chem Res*. 2011, 50, 6704–6712.
26. Song X.; Wang, W.; Yang, F.; Wang, G.; and Rui, X. The study of natural rubber/polybutadiene rubber hybrid matrix-based magnetorheological elastomer. . *J. Thermoplast. Compos. Mater.* 2022, 35, 17–35.
27. El-Sabbagh, S.; and Yehia, A. Detection of crosslink density by different methods for natural rubber blended with SBR and NBR. *Egypt J Solids.* 2007, 30, 157–173.

28. Pal, K.; Rajasekar, R.; Kang, D.; Zhang, Z.; Pal, S.; Das, C.; and Kim, J. Effect of Filler and Urethane Rubber on NR/BR with Nanosilica: Morphology and Wear. *J. Thermoplast. Compos. Mater.* 2010, 23. doi:10.1177/0892705709355234.
29. Ge, L.; Gong, X.; Fan, Y.; Xuan, S. Preparation and mechanical properties of the magnetorheological elastomer based on natural rubber/rosin glycerin hybrid matrix. *Smart Mater. Struct.* 2013, 11, 115029.
30. Rajamohan, V.; Sedaghati, R.; and Rakheja, S. Vibration analysis of a multi-layer beam containing magnetorheological fluid. *Smart Mater. Struct.* 2009, 19, 015013.
31. Rajamohan, V.; Sundararaman, V.; and Govindarajan, B. Finite element vibration analysis of a magnetorheological fluid sandwich beam. *Procedia Eng.* 2013, 64, 603–612.
32. Edwin Sudhagar, P., Ananda Babu, A., Vasudevan, R., and Jeyaraj, P. Vibration analysis of a tapered laminated thick composite plate with ply drop-offs. *Arch. Appl. Mech.* 2015, 85, 969-990.
33. Lee, J. Y.; Kumar, V.; and Lee, D.-J. Compressive properties of magnetorheological elastomer with different magnetic fields and types of filler. *Polym. Adv. Technol.* 2019, 30,1106–1115.
34. Fan, Y.; Gong, X.; Xuan, S.; Zhang, W.; Zheng, J.; and Jiang, W. Interfacial friction damping properties in magnetorheological elastomers. *Smart Mater. Struct.* 2011, 20, 035007.